RSC Advances

PAPER

View Article Online
View Journal | View Issue

Cite this: *RSC Adv.*, 2017, **7**, 54347

Biochemical, thermodynamic and structural studies of recombinant homotetrameric adenylosuccinate lyase from *Leishmania braziliensis*†

Luiza Galina,[ab] Pedro Ferrari Dalberto,[ab] Leonardo Kras Borges Martinelli,[a] Candida Deves Roth,[a] Antonio Frederico Michel Pinto,[a] Anne Drumond Villela,[a] Cristiano Valim Bizarro,[ab] Pablo Machado,[ab] Luis Fernando Saraiva Macedo Timmers,[bc] Osmar Norberto de Souza,[abc] Edgar Marcelino de Carvalho Filho,[d] Luiz Augusto Basso *[ab] and Diogenes Santiago Santos[ab]

Adenylosuccinate lyase (ASL) is involved in both *de novo* and salvage pathways of purine biosynthesis. ASL belongs to the argininosuccinate lyase/fumarase C superfamily of enzymes which share a general acid–base catalytic mechanism with β-elimination of fumarate as the common product. Cloning, expression, and a method to obtain homogeneous recombinant ASL from *Leishmania braziliensis* (*Lb*ASL) are described. Mass spectrometry analysis of recombinant *Lb*ASL, oligomeric state determination and multiple sequence alignment are presented. Steady-state kinetics of *Lb*ASL showed a Michaelis–Menten pattern. Isothermal titration calorimetry binding assays suggested that *Lb*ASL follows a Uni-Bi ordered kinetic mechanism, in which release of fumarate is followed by AMP to yield free enzyme. Initial velocity data for the reverse reaction and the Haldane relationship allowed calculation of an unfavorable equilibrium constant for the *Lb*ASL-catalyzed chemical reaction. The activation energy and thermodynamic activation parameters were estimated. Solvent kinetic isotope effects V/K and V suggest a modest contribution of solvent proton transference during the rate-limiting step of the reaction. Proton inventory data show that the modest normal effect on V arises from a single protonic site, and the transition state fractionation factor value of 0.74 suggests participation of solvent proton transfer in transition-state vibrations perpendicular to the reaction coordinate. pH-rate profiles for k_{cat} and k_{cat}/K_M suggested amino acid residues involved in, respectively, catalysis and substrate binding. A model of *Lb*ASL was built to provide a structural basis for the experimental data. A better understanding of the mode of action of *Lb*ASL is useful for the rational design of antileishmaniasis agents.

Received 22nd September 2017
Accepted 22nd November 2017

DOI: 10.1039/c7ra10526f

rsc.li/rsc-advances

Introduction

Leishmaniasis is regarded as one of the most burdensome of the neglected tropical diseases.[1] The disease is endemic in 98 countries and three continents, and it is estimated that 350 million people are at risk.[2] Approximately 0.2 to 0.4 million cases of visceral leishmaniasis (VL) and 0.7 to 1.2 million cases of cutaneous leishmaniasis (CL) occur each year. CL is more widely distributed, with about one-third of cases occurring in the Americas, the Mediterranean basin, and Western and Central Asia.[3] In Brazil, American tegumentary leishmaniasis (ATL) is predominantly caused by *Leishmania* (Viannia) *braziliensis*,[4] which is responsible for four distinct forms of ATL: localized CL, mucosal leishmaniasis (ML), disseminated leishmaniasis (DL) and diffuse CL (DCL).[5,6] Like other *Leishmania* species, *L. braziliensis* is a digenetic protozoan parasite that is a flagellated, extracellular promastigote in the phlebotomine sandfly vector, while it is an immotile, intracellular amastigote within phagolysosomes of macrophages of the infected mammalian host.[4] The main drug treatments of leishmaniasis include pentavalent antimonials, like sodium stibogluconate (Pentostam) and meglumine antimoniate (Glucantime) (Croft *et al.* 2011, Croft *et al.* 2003; McGwire 2014). However, these antimonials have multiple toxicities and are increasingly

[a]*Centro de Pesquisas em Biologia Molecular e Funcional (CPBMF), Instituto Nacional de Ciência e Tecnologia em Tuberculose (INCT-TB), Pontifícia Universidade Católica do Rio Grande do Sul (PUCRS), 6681/92-A, TecnoPuc, Av. Ipiranga 6681, 90619-900, Porto Alegre, RS, Brazil. E-mail: luiz.basso@pucrs.br; Fax: +55-51-33203629; Tel: +55-51-33203629*

[b]*Programa de Pós-Graduação em Biologia Celular e Molecular, PUCRS, Porto Alegre, RS, Brazil*

[c]*Laboratório de Bioinformática, Modelagem e Simulação de Biossistemas (LABIO), Pontifícia Universidade Católica do Rio Grande do Sul (PUCRS), Av. Ipiranga 6681, 90619-900, Porto Alegre, RS, Brazil*

[d]*Hospital Universitário Professor Edgard Santos, Universidade Federal da Bahia, Salvador 40110160, BA, Brazil*

† Electronic supplementary information (ESI) available. See DOI: 10.1039/c7ra10526f

ineffective due to the development of parasite resistance.[7–9] Although second-line drugs, such as amphotericin-B either as deoxycholate or liposomal form, paromomycin and miltefosine show fewer side effects;[7,10] these therapies are very expensive and are far from ideal.[11] There is thus an urgent need for new treatments to combat this disease.

The development of new effective antiparasitic drugs can be based on exploring the biochemical and physiological differences between the pathogen and its host. One of these metabolic differences lies in the biosynthesis of purine nucleotides.[12,13] While mammal cells hold the capacity to synthetize purine nucleotides by the *de novo* and salvage pathways, *Leishmania* species are completely dependent on the salvage pathway to supply their purine requirements.[14,15] The enzyme adenylosuccinate lyase (ASL; EC 4.3.2.2) belongs to the aspartase/fumarase protein superfamily, all members of which are homotetramers with approximately 200 kDa that share a high level of structural similarity.[16–19] ASL is the only enzyme in the purine nucleotide metabolism that catalyzes two distinct reactions, both involving β-elimination of fumarate: (1) conversion of 5-aminoimidazol-4(*N*-succinylcarboxamide) ribonucleotide (SAICAR) into 5-aminoimidazole-4-carboxamide ribonucleotide (AICAR) and fumarate, and (2) conversion of succinyl-adenosine monophosphate (S-AMP) into AMP and fumarate. The latter reaction is part of the two-reaction pathway that converts inosine monophosphate (IMP) into AMP.[16] ASL is the last enzyme in the conversion of IMP to AMP in *Leishmania*, representing therefore a critical bottleneck in purine salvage (Boitz *et al.* 2013). Previous studies showed that an *L. donovani* parasite containing the ASL gene knocked-out exhibited a severely reduced parasite burden in both macrophages and mice, which could be explained by the toxic accumulation of adenylosuccinate.[13] These results indicate that ASL could be a promising drug target for anti-leishmaniasis drug development.

Here, we describe cloning, expression and purification to homogeneity of recombinant *L. braziliensis* ASL (*Lb*ASL). Determination of the true steady-state kinetic parameters, thermodynamic constants of substrate and products interaction, pre-steady-state kinetics, energy of activation, solvent kinetic isotope effect (SKIE) and proton inventory studies are also presented. A three-dimensional model has been built to provide a structural basis for interpretation of experimental results. These results contribute to a better understanding of the mode of action of *Lb*ASL, which should inform the rational design of chemotherapeutic agents to treat leishmaniasis.

Experimental

Materials

All chemicals were of analytical or reagent grade and were used without further purification, unless stated otherwise. Buffers, S-AMP, AMP, fumarate, ammonium sulfate, streptomycin sulphate, sodium chloride, potassium chloride, EDTA, DTT, glycerol, D_2O and lysozyme were purchased from Sigma Aldrich® (Saint Louis, USA). Bacterial growth media and antibiotics were from Gibco. Liquid chromatography columns, low molecular weight (LMW) and high molecular weight (HMW) Gel Filtration Calibration Kits were purchased from GE Healthcare® Life Sciences (Pittsburg, USA). All kinetic data analyses were carried out using SigmaPlot 10.0 (Systac Software, Inc., Melbourne, USA). Data are presented as mean ± standard deviation unless stated otherwise. ITC data analysis was evaluated utilizing the Origin 7 SR4 software (Microcal, Inc.). All enzyme activity measurements were carried out at 25 °C in at least duplicates.

Cloning and recombinant protein expression

The *Lb*ASL coding gene *Lb*rM.04.0500 (GenBank ID: 5412684) containing *Nde*I and *Hind*III restriction sites on, respectively, the 5′ and 3′ ends was synthetized with signal peptide removed by Biomatik® and ligated into the pET23a(+) expression vector pET23a(+):*Lb*rM.04.0500, previously digested with the same restriction enzymes. The construction of pET23-a(+):*Lb*rM.04.0500 was submitted to automatic DNA sequencing to confirm identity, integrity and absence of mutations in the cloned gene.

The recombinant plasmid pET23a(+):*Lb*rM.04.0500 was transformed into *E. coli* BL21(DE3) cells and plated on lysogeny broth (LB) agar containing 50 μg mL^{-1} ampicillin. A single colony was inoculated into *LB* medium (50 mL) containing 50 μg mL^{-1} ampicillin and grown at 37 °C, 180 rpm, overnight. The culture (8.5 mL) was inoculated in LB medium (500 mL) with the same antibiotic concentration and grown in a shaker-incubator at 37 °C, 180 rpm. When the optical density at 600 nm (OD_{600}) reached 0.4–0.6, as suggested by New England BioLabs Inc[20] and previous reports,[21,22] the cells were induced with 1 mM of isopropyl β-D-1-thiogalactopyranoside (IPTG) and harvested at 3 h, 6 h, 9 h, 12 h and 24 h after induction. Cells were harvested by centrifugation at 8000 × *g*|*g* for 30 min at 4 °C and stored at −20 °C. Frozen cell paste was disrupted by sonication and soluble and insoluble fractions were analyzed by 12% sodium dodecyl sulfate polyacrylamide gel electrophoresis (SDS-PAGE).

Protein purification

Protein purification was performed by FPLC using an ÄKTA System (GE Healthcare® Life Sciences, Pittsburg, USA) at 4 °C. Approximately 1.8 g of frozen cells were suspended in 9 mL of 50 mM Tris HCl pH 7.5 (buffer A), and incubated with 0.2 mg mL^{-1} lysozyme (Sigma-Aldrich) with stirring for 30 min at 4 °C. Cells were disrupted in a VCX 750 ultrasonic processor (Sonics & Materials Inc., Newtown, USA) by sonication (10 pulses of 10 s each at 60% amplitude) and centrifuged at 48 000 × *g*|*g* for 30 min at 4 °C. The supernatant was treated with 1% (v/v) streptomycin sulfate for 30 min with slow stirring to precipitate nucleic acids and centrifuged at 48 000 × *g*|*g* for 30 min at 4 °C. The resulting supernatant was treated with 1.5 mM ammonium sulfate with stirring for 30 min. The fraction containing precipitated molecules was suspended with 8 mL of buffer A and loaded on a HiLoad Superdex 200 26/60 size exclusion column (GE Healthcare® Life Sciences, Pittsburg, USA), previously equilibrated with buffer A. Proteins were

isocratically eluted with 1 column volume (CV) of buffer A at flow rate of 0.5 mL min^{-1}, and fractions containing the target protein were pooled and loaded on a HiLoad Q Sepharose High Performance 16/10 anion exchange column (GE Healthcare® Life Sciences, Pittsburg, USA), pre-equilibrated with buffer A. The column was washed with 7 CVs of buffer A, and the adsorbed proteins were eluted with a linear gradient (0–60%) of 25 CV of buffer A containing 1 M NaCl (buffer B) at flow rate of 1 mL min^{-1}. The fractions containing homogeneous *Lb*ASL were pooled and dialyzed against 50 mM potassium phosphate buffer pH 7.0, containing 150 mM KCl, 1 mM EDTA, 1 mM DTT and 10% glycerol (storage buffer), and stored at −20 °C. Protein concentration was determined by the method of BCA using a bovine serum albumin as standard (BCA protein Assay Kit, Thermo Scientific Pierce).

LbASL identification by mass spectrometry

The homogeneous protein was submitted to shotgun proteomics to confirm the enzyme's identity. In-gel digestion was performed according to Shevchenko *et al.*[23] Tryptic digest of *Lb*ASL was separated on a homemade 20 cm reverse-phase column (5 μm ODSAQ C18, Yamamura Chemical Lab, Japan) using a nanoUPLC (nanoLC Ultra 1D plus, Eksigent, USA) and eluted directly to a nanospray ion source connected to a hybrid mass spectrometer (LTQ Orbitrap Discovery, Thermo, USA). The flow rate was set to 300 mL min^{-1} in 120 min reverse-phase gradient. The mass spectrometer was operated in a data-dependent mode, with full MS1 scan collected in the Orbitrap, with m/z range of 400–1600 at 30 000 resolution. The eight most abundant ions per scan were selected to CID MS2 in the ion trap. Mass spectra were analyzed using PatternLab platform.[24] MS2 spectra were searched with COMET[25] using a non-redundant database containing forward and reverse *E. coli* DH10B reference proteome and the sequence of *Lb*ASL. The validity of the peptide-spectra matches (PSMs) generated by COMET was assessed using PatternLab's module SEPro with a false discovery rate of 1% based on the number of decoys.

Oligomeric state determination

An estimate for the molecular mass of *Lb*ASL in solution was obtained by injecting 100 μL of protein suspension (7 μM homogeneous *Lb*ASL in 50 mM Tris HCl pH 7.5 containing 200 mM NaCl) into a HighLoad 10/30 Superdex-200 column (GE Healthcare), and isocratically eluted with 1 CV of 50 mM Tris HCl pH 7.5 containing 200 mM of NaCl at 0.4 mL min^{-1}.

Protein elution was monitored at 215, 254 and 280 nm. The low molecular weight (LMW) and high molecular weight (HMW) Gel Filtration Calibration Kits (GE Healthcare) were used to prepare a calibration curve, measuring the elution volumes (V_e) of several standards (ferritin, aldolase, ovalbumin, conalbumin, ribonuclease and carbonic anhydrase A). These values were used to calculate their partition coefficient (K_{av}, eqn (1)). Blue dextran 2000 (GE Healthcare) was used to determine the void volume (V_0). V_t is the total bead volume of the column. The K_{av} value for each protein was plotted against their correspondent molecular mass to obtain an estimate for *Lb*ASL molecular mass in solution.

$$K_{AV} = \frac{V_e - V_0}{V_t - V_0} \quad (1)$$

Multiple sequence alignment and homology modeling

Multiple alignment was carried out to compare amino acid sequences of homologous ASL proteins whose residues in the active site were determined by mutagenesis studies or for which three-dimensional structures were solved. The following proteins were included in the alignment: *Leishmania braziliensis* (*Lb*ASL, XP_001561734), *Leishmania donovani* (*Ld*ASL, XP_003858107), *Escherichia coli* (*Ec*ASL, WP_000423742), *Plasmodium falciparum* (*Pf*ASL, XP_001349577), *Bacillus subtilis* (*Bs*ASL, WP_003233955), *Homo sapiens* (*Hs*ASL, NP_000017), and *Mycobacterium tuberculosis* (*Mt*ASL, WP_003898583). The alignment was performed by ClustaW[26] using the Blosum62 matrix.

The homology modelling approach, implemented in the MODELLER[27] 9v19 program, was used to build a 3D model of *Lb*ASL. The structure of ASL from *E. coli* (PDB ID: 2PTQ) associated with the products AMP and fumarate was used as template. This template was selected because the presence of products in the enzyme's active site provides structural information on which to base interpretation of the pH-rate profile data. The protocol used to perform the molecular modelling experiments generated 10 models. All models were submitted to the DOPE energy scoring function[28] implemented in the MODELLER 9v19 aiming to select the best structures. The MOLPROBITY webserver[29] and PROCHECK[30] were used to verify and validate the stereochemical quality of the models.

Steady-state kinetic parameters of *Lb*ASL

Recombinant *Lb*ASL enzyme activity was monitored by a continuous assay in a UV-2550 UV/visible spectrophotometer (Shimadzu) equipped with a temperature-controlled cuvette holder, using 1.0 cm path length quartz cuvettes. The kinetic data were determined using the difference in absorption between S-AMP and AMP and fumarate, measuring the decrease in absorbance at 282 nm using a difference extinction coefficient value of 10 000 M^{-1} cm^{-1}. One unit of enzyme activity (U) was defined as the amount of enzyme catalyzing the conversion of 1 μmol of substrate into products per second at 25 °C. The enzyme was pre-incubated for 30 min at 25 °C in storage buffer. All enzyme activity assays were performed at 25 °C in 50 mM Tris HCl pH 7.5 containing 200 mM NaCl and 5 mM EDTA (buffer C) (standard conditions), in a total volume of 0.5 mL and reaction course data collected for 60 s. Only for the Superdex 200 eluate step enzyme activity was monitored for 5 min. For the purification steps, S-AMP substrate concentration was fixed at 100 μM (saturation), whereas initial velocity studies employed variable concentrations as described in the next paragraph.

The initial velocity study was carried out to determine the steady-state kinetic parameters for S-AMP conversion into AMP and fumarate (forward reaction). The saturation curve was performed at varying concentrations of S-AMP (5–200 μM) and

the reaction was initiated by the addition of 30 nM of recombinant *Lb*ASL. Hyperbolic saturation curves were analyzed by non-linear regression of data fitting to the Michaelis–Menten equation (eqn (2)), in which v is the steady-state velocity, V is the maximal velocity, A is the substrate concentration, and K_M is the Michaelis–Menten constant.

$$v = \frac{VA}{K_M + A} \quad (2)$$

The k_{cat} values were calculated from eqn (3), in which $[E]_t$ corresponds to the total concentration of enzyme subunits.

$$k_{cat} = \frac{V}{[E]_t} \quad (3)$$

The initial velocities for the reverse reaction were determined varying the concentration of AMP (10–800 μM) at varied-fixed fumarate concentration (100–900 μM). All reactions started with addition of recombinant *Lb*ASL, assayed under standards conditions, and all measurements were performed at least in duplicates. Data from initial velocity measurements showing a pattern of lines intersecting to the left of the y-axis in the double-reciprocal plots (or Lineweaver–Burk plots) were fitted to eqn (4), which describes a sequential substrate binding and ternary complex formation (reverse reaction).

$$v = \frac{VAB}{K_{ia}K_b + K_aB + K_bA + AB} \quad (4)$$

For eqn (4), v is the initial velocity, V is the true maximal initial velocity, A and B are the concentrations of the substrates (AMP and fumarate) for the reverse reaction, $K_a(K_q)$ and $K_b(K_p)$ are their respective Michaelis–Menten constants, and $K_{ia}(K_{iq})$ is the dissociation constant for enzyme–substrate A binary complex formation (enzyme–AMP binary complex formation for the reverse reaction).

The initial velocities for the reverse reaction were employed to calculate the equilibrium constant (K_{eq}) using the Haldane equation for an ordered Uni-Bi (or Bi-Uni) mechanism (eqn (5)). V_f is the maximal initial velocity for the forward and V_r for the reverse reaction, K_p represents the Michaelis–Menten constant for the first product to be released from the ternary complex (fumarate), K_a represents the Michaelis–Menten constant for S-AMP (K_M of eqn (2)), and K_{iq} represents the dissociation constant for enzyme–AMP binary complex formation for the reverse reaction.[31]

$$K_{eq} = \frac{V_fK_{iq}K_p}{V_rK_a} \quad (5)$$

Isothermal titration calorimetry (ITC)

ITC experiments were carried out using an iTC_{200} Microcalorimeter (Microcal, Inc., Northampton, MA). The reference cell (200 μL) was loaded with water during all the experiments and the sample cell (200 μL) was filled with recombinant *Lb*ASL at a concentration of 72 μM in buffer C. The injection syringe (39.7 μL) was filled with either AMP (2 mM) or fumarate (2 mM) in the same buffer, and the ligand binding isotherms were measured by direct titration (ligand into macromolecule). The stirring speed was 500 rpm at 25 °C and constant pressure. Titration first injection (0.5 μL) was not used in data analysis and was followed by 19 injection of 2 μL each at 300 s intervals. Control titrations (ligand into buffer) were performed in order to subtract the heats of dilution prior to data analysis. The Gibbs free energy (ΔG) of binding was calculated using the relationship described in eqn (6), in which R is the gas constant (1.987 cal K^{-1} mol^{-1}), T is the temperature in Kelvin (T = °C + 273.15), and K_a is the association constant at equilibrium. The entropy of binding (ΔS) can also be determined by this mathematical formula. ΔH represents the enthalpy of binding. The dissociation constant at equilibrium, K_d, was calculated as the inverse of K_a (eqn (7)). All data were evaluated utilizing the Origin 7 SR4 software (Microcal, Inc.)

$$\Delta G^0 = -RT \ln K_a = \Delta H^0 - T\Delta S^0 \quad (6)$$

$$K_d = \frac{1}{K_a} \quad (7)$$

Energy of activation

To determine the energy of activation (E_a) of *Lb*ASL for the forward reaction, the dependence of k_{cat} on temperature was measured. Initial velocities were measured in the presence of saturating concentrations of S-AMP (100 μM) at temperatures varying from 15 to 40 °C (from 288.15 to 313.15 K). Prior to data collection, *Lb*ASL was incubated for several minutes at all tested temperatures and assayed under standards conditions to ascertain enzyme stability is maintained. All assays were performed in duplicates. E_a was calculated from the slope (E_a/R) of the Arrhenius plot fitting the data to eqn (8), in which R is the gas constant (8.314 J mol^{-1} K^{-1}), and A is the Arrhenius constant, which represents the product of the collision frequency (Z), and a steric factor (p) based on the collision theory of enzyme kinetics.[32,33] A simplistic approach was adopted to explain a complex phenomenon and that A is independent of temperature.

$$\ln k_{cat} = \ln A - \left(\frac{E_a}{R}\right)\frac{1}{T} \quad (8)$$

The E_a value allowed to obtain an estimate for the enthalpy of activation ($\Delta H^{\#}$) employing eqn (9). The Gibbs free energy ($\Delta G^{\#}$) of activation was estimated using eqn (10). These values allowed to obtain an estimate for the entropy of activation ($\Delta S^{\#}$) using eqn (11). These equations were derived from the transition state theory of enzymatic reactions.32,33 R, E_a and T are as for eqn (8), k_b is the Boltzmann constant (1.380658×10^{-23} J K^{-1}), and h is the Planck's constant (6.626075×10^{-34} J s^{-1}). The error in $\Delta G^{\#}$ was calculated using eqn (12).

$$\Delta H^{\#} = E_a - RT \quad (9)$$

$$\Delta G^{\#} = RT\left(\ln\frac{k_B}{h} - \ln T - \ln k_{cat}\right) \quad (10)$$

$$\Delta S^{\#} = \frac{\Delta H^{\#} - \Delta G^{\#}}{T} \quad (11)$$

$$\left(\Delta G^{\#}\right)_{Err} = \frac{RT(k_{cat})_{Err}}{k_{cat}} \quad (12)$$

Solvent kinetic isotope effects (SKIE) and proton inventory

All assays were carried out under standard reaction conditions, in duplicate. The solvent kinetic isotope effects on both V/K and V were determined by measuring initial velocities for *Lb*ASL reaction using varied concentrations of S-AMP in either H_2O or 90% D_2O. The SKIE data were fitted to eqn (13),[34] in which V is the maximal velocity, A is the substrate concentration, $E_{V/K}$ and E_V are, respectively, the isotope effect minus 1 on V/K and V, and F_i is the fraction of deuterium label in the solvent.

$$v = \frac{VA}{K(1 + F_iE_{V/K}) + A(1 + F_iE_V)} \quad (13)$$

To determine the number of protons contributing to the observed solvent kinetic isotope effect, the proton inventory on the catalytic rate constant (k_{cat}) was measured at saturating concentration of S-AMP at different mole fractions of D_2O (0–90%). The data for the relative activity *versus* mole fraction of D_2O plot were fitted to the Gross–Butler equation (eqn (14)),[34] in which k_n is the rate constant measured at various mole fractions of D_2O (*e.g.*, $k_0 = k_{cat}$ value in H_2O, and $k_{0.9} = k_{cat}$ value in 90% D_2O), n is the isotopic composition of the solvent, and ϕ^T is the deuterium fractionation factor for transition-state proton exchange relative to bulk water (*i.e.*, exchange equilibrium constant that measures the tendency of a transition-state site to fractionally contain deuterium *versus* the deuterium fraction of the solvent). It should be pointed out that eqn (14) implies that a single proton contributes to the observed solvent isotope effect and that the reactant-state fractionation factor is equal to unity.

$$\frac{k_n}{k_0} = 1 - n + n\phi^T \quad (14)$$

pH-rate profiles

Prior to carrying out pH-rate studies, *Lb*ASL was incubated for 2 min at 25 °C in 100 mM 2-(*N*-morpholino)-ethanesulfonic acid (MES)/*N*-2-hydroxyethylpiperazine-*N*-2-ethanesulfonic acid (Hepes)/2-(*N*-cyclohexylamino)-ethanesulfonic acid (CHES) buffer mixture over a wide pH range (5.0–10.5),[35] and assayed under standard conditions to ensure enzyme stability at the experimental pH values over the course of reaction, thereby showing that changes in enzyme activity were due to changes in proton concentration and not to protein denaturation. Initial velocities measurements were carried out at 25 °C in solutions containing increasing concentrations of S-AMP in 100 mM MES/HEPES/CHES buffer mixture over the following pH values: 6.3 (S-AMP concentration range: 40–150 μM, [*Lb*ASL] = 60 nM), 6.5 (S-AMP concentration range: 5–60 μM with 6 or 12 nM of *Lb*ASL), 6.7 (S-AMP concentration range: 1–60 μM with 6 or 12 nM of *Lb*ASL), 7.0 (S-AMP concentration range: 5–60 μM with 6 or 12 nM of *Lb*ASL), 7.5 (S-AMP concentration range: 3–60 μM with 6 or 12 nM of *Lb*ASL), 8.0 (S-AMP concentration range: 5–60 μM with 6 or 12 nM of *Lb*ASL), 8.5 (S-AMP concentration range: 20–180 μM with 6 or 12 nM of *Lb*ASL), 9.0–9.5 (S-AMP concentration range: 20–200 μM, [*Lb*ASL] = 12 nM). The pH-rate data for k_{cat} (Fig. 10A) were plotted to eqn (15), in which y represents k_{cat}, C is the pH-independent plateau value of $y(k_{cat})$, H is the hydrogen ion concentration, and K_a and K_b are, respectively, the apparent acid and base dissociation constant for the ionizing group. Eqn (15) describes a bell-shaped pH profile for a group that must be protonated for catalysis and another group that must be unprotonated for catalysis, and participation of a single ionizing group for the acidic limb (slope value of +1) and participation of a single ionizing group for the basic limb (slope value of −1).[35]

$$\log y = \log\left(\frac{C}{1 + \frac{H}{K_a} + \frac{K_b}{H}}\right) \quad (15)$$

The pH-rate profile for k_{cat}/K_M was more complex (Fig. 10B). The data were tentatively either fitted to eqn (15) or (16). The latter equation describes a bell-shaped pH profile that starts with a slope of +2 in the acidic limb which goes to an eventual slope of −1 in the basic limb, suggesting participation of two ionizing groups in the acidic limb.[35] K_0 is the product of two apparent dissociation constants. Unless the pKs of the groups are at least 3 pH units apart, there will not be both a linear region with a slope of +1 and a flat plateau at intermediate pH values. The intersection of the linear asymptote with slope of 2 and the poorly defined plateau will give the average of the pK values of the two ionizing groups.[35]

$$\log y = \log\left(\frac{C}{1 + \frac{H}{K_a} + \frac{H^2}{K_0} + \frac{K_b}{H}}\right) \quad (16)$$

Results and discussion

Cloning and recombinant protein expression

The *Lb*ASL-coding DNA sequence *Lb*rM.04.0500 was purchased from Biomatik® and cloned into the pET-23a(+) expression vector. Automated DNA sequencing confirmed the identity and the absence of mutations in the cloned fragment. The best experimental condition for *Lb*ASL protein expression was observed in competent *E. coli* BL21 (DE3) cells, in *LB* medium after 12 h of growth, without IPTG induction. SDS-PAGE analysis showed that the protein was expressed in the soluble fraction of cellular extracts (~51 kDa) which is in agreement with the predicted molecular mass value of 51.269 kDa for *Lb*ASL subunit. The expressed recombinant *Lb*ASL protein was purified to homogeneity (ESI, Fig. S1†). The protein purification protocol

(streptomycin sulfate and ammonium sulfate precipitations, and size exclusion and anion exchange columns) yielded approximately 19 mg from 1.8 g of frozen cells indicating a protein yield of 40% (ESI, Table S1†). The recombinant protein was stored at −20 °C in the storage buffer (50 mM potassium phosphate buffer pH 7.0, 150 mM KCl, 1 mM EDTA, 1 mM DTT and 10% glycerol). The storage buffer was identified as the best condition to maintain enzyme stability for up to 3 months. The recombinant enzyme lost more than 50% of initial activity after 3 months when stored at either −20 °C or −80 °C.

*Lb*ASL identification by mass spectrometry

The gel band of approximately 51 kDa was excised from SDS-PAGE, submitted to trypsin digestion protocol, and the peptides were analyzed by LC-MS/MS in triplicate. *Lb*ASL identity was confirmed, with the identification of 189 unique peptides and sequence coverage of 100% (ESI, Fig. S2†).

Oligomeric state determination

To determine the oligomeric state of recombinant *Lb*ASL, 100 μL was loaded on a Superdex 200 HR 10/30 size exclusion column. A single peak was obtained with elution volume corresponding to approximately 223 357 kDa, according to data fitting to eqn (1) (ESI, Fig. S3†). This molecular mass value divided by the subunit molecular mass value (51.2699 kDa) indicates that *Lb*ASL is a homotetramer in solution. This result is in agreement with the ASL characterized previously from human,[36] *L. donovani*[13] and others aspartase/fumarase superfamily members.[19]

Multiple sequence alignment and homology modeling

The multiple sequence alignment for *Leishmania braziliensis* (*Lb*ASL), *Leishmania donovani* (*Ld*ASL), *Escherichia coli* (*Ec*ASL), *Plasmodium falciparum* (*Pf*ASL), *Bacillus subtilis* (*Bs*ASL),[18,37,38] *Homo sapiens* (*Hs*ASL), and *Mycobacterium tuberculosis* (*Mt*ASL),[39] allowed to propose the likely amino acid residues involved in *Lb*ASL catalysis and substrate binding (Fig. 1). Multiple sequence alignment results showed that *Lb*ASL shares 88%, 45%, 35%, 18%, 17% and 12% sequence identity with, respectively, *L. donovani*, *E. coli*, *Plasmodium falciparum*, *B. subtillis*, *H. sapiens* and *M. tuberculosis*.

The general mechanism proposed for ASL catalysis is a β-elimination (anti 1,2-addition-elimination reaction), in which a general base of the enzyme abstracts the *pro-R* hydrogen from the C3 atom (Cβ) of the succinyl moiety of the substrate.[40] The resulting carbanion is stabilized as the aci-carboxylate (or enediolate) intermediate with two negative charges on the β-carboxylate group. Cleavage of the C–N bond of the substrate is assisted by leaving group protonation by an enzyme general acid.[19] As the reaction occurs *via* anti elimination, two separate amino acid residues for proton abstraction and donation are required. Conserved His^{141} and His^{68} in *B. subtilis* have been proposed to be, respectively, the base and acid groups.[37,41] The sequence comparison showed that residues equivalent to these histidines are conserved (Fig. 1), suggesting that His^{197} and/or His^{119} may play a role in *Lb*ALS catalysis. Alternatively, the catalytic base residue may be ascribed to Ser^{322} in *Lb*ASL (Fig. 1). Proteins belonging to the aspartase/fumarase superfamily (including ASL) share a characteristic tertiary and quaternary fold as well as similar active site architecture.[19] The monomer is comprised of three mainly α-helical domains: N-terminal (D1), central helix (D2) and C-terminal (D3). Three conserved regions are found in the D2 domain: C1 located at the start of D2, and C2 and C3 that are located in the loop regions between the helices of D2 (Fig. 2). Although spatially separated in the monomeric unit, the C1–C3 domains from three different subunits form the active site of the tetrameric protein (Fig. 2). Part of the conserved C3 region is formed by the flexible Ser–Ser loop, which undergoes conformational changes upon substrate binding that is relevant to catalysis in ASL enzymes.[42,43] The signature sequence of this Ser–Ser loop in *Lb*ASL is 321GSSXXPXKXN330, and is highly conserved among all aligned sequences (Fig. 1). Site-directed mutagenesis studies on *B. subtilis* indicated that Gln^{212}, Asn^{270}, and Arg^{301} residues perform critical functions in catalysis by ASL through their contributions to the binding and orientation of the succinyl carboxylate groups of its two substrates SAICAR and S-AMP.[34] The corresponding Gln^{274}, Asn^{330} and Arg^{362} residues in *Lb*ASL are also conserved in the ASLs from other organisms (Fig. 1), except Arg^{362} that is replaced with a glycine in *M. tuberculosis*.[39]

The homology model of *Lb*ASL (Fig. 3) shows a His^{197} at 4.1 Å of the C–N bond of AMP, suggesting that this residue may act as the catalytic acid. The conserved Ser^{322} is in close proximity (2.9 Å) to the C(β or α)-H bond of fumarate. This serine is in the highly conserved flexible Ser–Ser loop, which closes the active site upon substrate binding. Accordingly, Ser^{322} side chain may act as the catalytic base in the *Lb*ASL reaction. Although it is tempting to suggest that the corresponding residues may play a role in *Lb*ASL mode of action, site-directed mutagenesis efforts will have to be pursued to assign any role to these amino acids.

The high conservation of key amino acid residues essential for substrate binding and catalysis for both *H. sapiens* and *L. braziliensis* ASL enzymes suggest that the development of selective inhibitors for *Lb*ASL might be challenging. Notwithstanding, a better understanding of the mode of action of *Lb*ASL may unveil differences in enzyme, chemical and catalytic mechanisms that may contribute to the development of mechanism-based anti-leishmaniasis agents.

Steady-state kinetic parameters

The initial velocity experiments were measured to obtain the true steady-state kinetics parameters and to propose an enzyme mechanism. It has been shown that *B. subtilis* ASL dissociates into a mixture of monomer–dimer–trimer with decreased enzyme activity at low temperatures (4 and 8 °C), whereas the enzyme is fully active and exists as 100% tetramer at 25 °C.[18] Accordingly, recombinant *Lb*ASL protein was pre-incubated for 30 min at 25 °C to ascertain maintenance of fully active tetrameric enzyme. Data for liquid chromatography carried out in a cold-room (~6 °C) using size exclusion column suggested that recombinant *Lb*ASL is homotetrameric (Fig. S3†). However, it should be pointed out that whether or not the

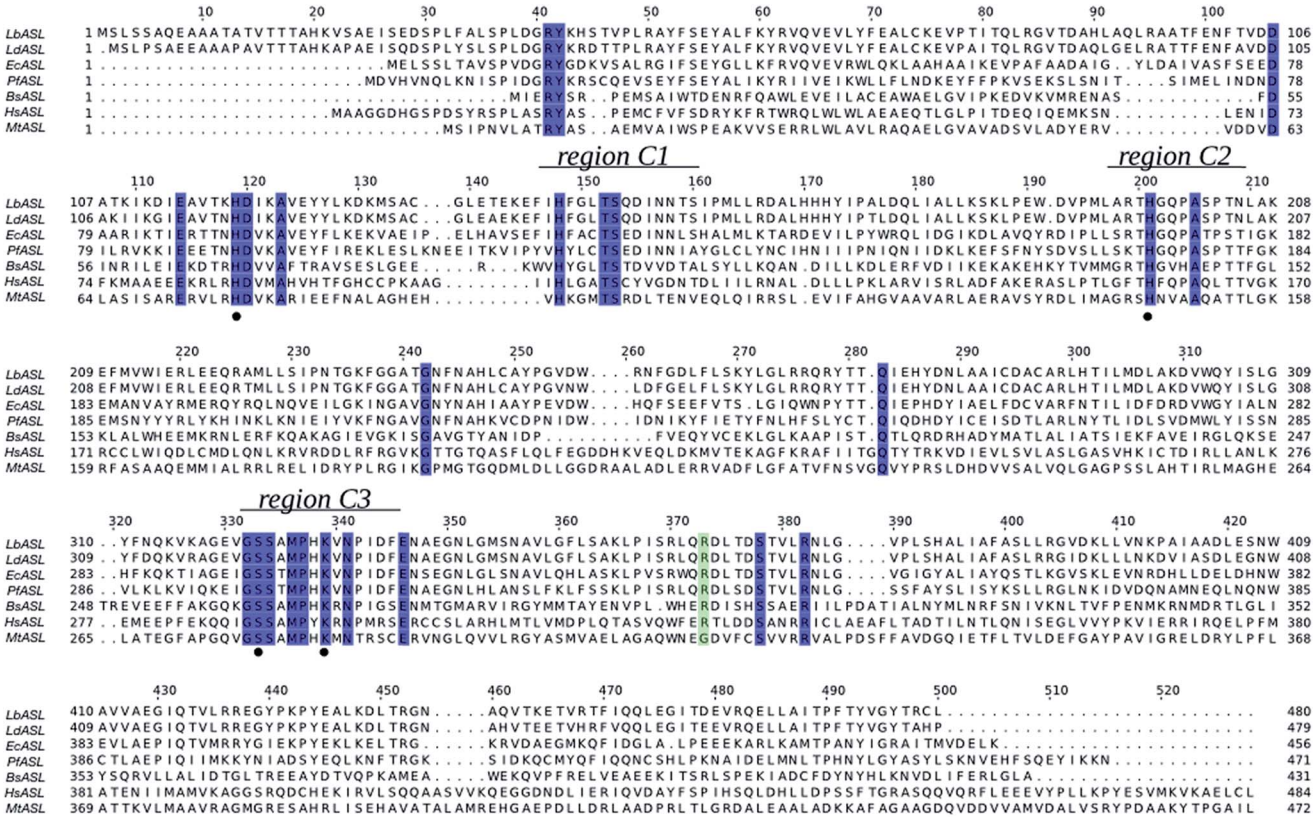

Fig. 1 Multiple sequence alignment of ASL from *Leishmania braziliensis* (*Lb*ASL, XP_001561734), *Leishmania donovani* (*Ld*ASL, XP_003858107), *Escherichia coli* (*Ec*ASL, WP_000423742), *Plasmodium falciparum* (*Pf*ASL, XP_001349577), *Bacillus subtilis* (*Bs*ASL, WP_003233955), *Homo sapiens* (*Hs*ASL, NP_000017), and *Mycobacterium tuberculosis* (*Mt*ASL, WP_003898583). Residues His119, His197, S322, and K328, proposed to be involved in catalysis, are indicated by black solid circles. ASL enzymes present three highly conserved regions, C1, C2, and C3 (residues 147–158, 194–204, and 321–331 in *Lb*ASL), which in the structure pack together to form the active site. The blue boxes represent residues conserved in all sequences. The green box represents residues conserved in all sequences, except in *Mycobacterium tuberculosis*. The alignment was prepared with ClustalW[26] and JalView.[56]

oligomeric state of *Lb*ASL changes as a function of temperature has to await analytical ultracentrifugation data. The specific activity of *Lb*ASL was obtained by varying the concentration of S-AMP (5–200 μM) and fixed concentration of enzyme (30 nM), and measuring the decrease in absorbance at 282 nm upon S-AMP conversion into products. Substrate saturation curves were hyperbolic (Fig. 4) and the data were thus fitted to the Michaelis–Menten equation (eqn (2)), and k_{cat} value was calculated using eqn (3). The hyperbolic profile suggests that there is no inhibition for S-AMP at 200 μM (~10-fold K_M). This analysis yielded the following steady-state kinetic parameters: $K_M = 11.1$ (±0.9) μM, $V_{max} = 6.4$ (±0.1) U mg^{-1} and $k_{cat} = 337$ (±5.4) s^{-1}. A comparison of the specific activity of ASL from *L. donovani*,[13,43] *P. falciparum*,[44] *H. sapiens*[36] and *M. smegmatis*[39] are summarized in Table 1. *Lb*ASL displays higher k_{cat} and specificity constant (k_{cat}/K_M) values in comparison to ASL enzymes from different species of *Leishmania* (Table 1). Interestingly, the larger overall dissociation constant (K_M) for S-AMP substrate of *Lb*ASL as compared to *H. sapiens* ASL may suggest differences from substrate binding en route to product formation that may be exploited to increase inhibitor specificity.

Double-reciprocal plots showed a family of lines intersecting to the left of the *y*-axis (Fig. 5), suggesting ternary complex formation and a sequential (either random or ordered) mechanism for the reverse reaction. The pattern of straight lines intersecting to the left of the *y*-axis rules out ping-pong (parallel lines), steady-state random (that gives non-linear reciprocal plots), and rapid-equilibrium ordered (one of the family of lines should cross at a single value on the *y*-axis) mechanisms. Accordingly, the data were fitted to eqn (4) yielding the following values: $K_{M(AMP)} = 13$ (±5) μM and $K_{M(fumarate)} = 203$ (±20) μM, $K_{i(AMP)} = 112$ (±20) μM, and $k_{cat} = 115$ (±3) s^{-1}. The steady-state kinetic parameters for the forward and reverse reactions and the Haldane equation for an ordered Uni-Bi mechanism (eqn (5)) were used to calculate a value of 5720 ± 1041 μM (*ca.* 5.7×10^{-6} M) for the equilibrium constant (K_{eq}). This result suggests that the forward reaction is not favorable under the *in vitro* experimental conditions here employed. However, the depletion of products in the physiological context may drive the reaction forward. At any rate, the double-reciprocal plots alone cannot distinguish between rapid-equilibrium random and steady-state compulsory ordered Uni-Bi mechanisms. ITC studies were thus performed to distinguish between these enzyme mechanisms.

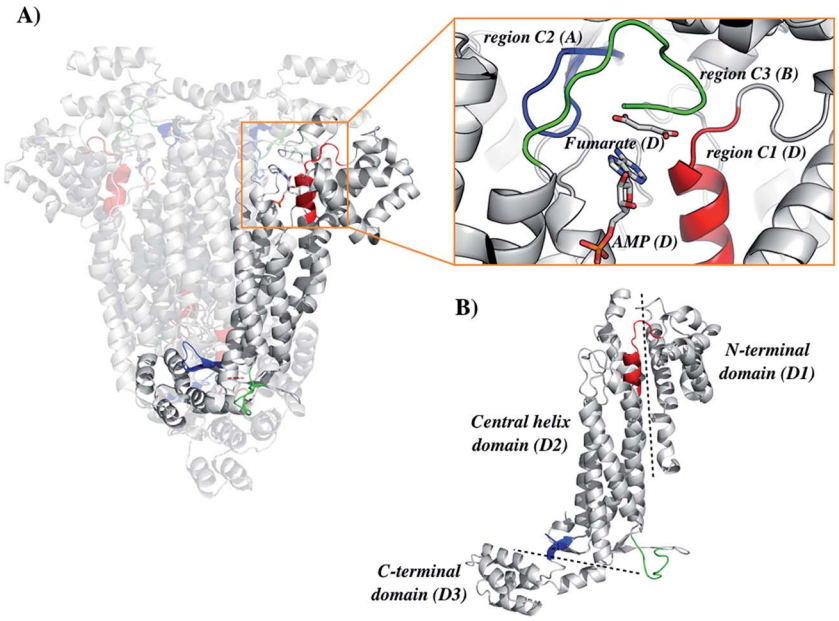

Fig. 2 Structure organization of the ASL from *Leishmania braziliensis* (*Lb*ASL). *Lb*ASL is biologically active as a homotetramer and contains four active sites. Amino acid residues of three subunits contribute to each enzyme active. (A) Quaternary structure of *Lb*ASL and a close view of the active site, which is formed by tight packing of regions C1 (red), C2 (blue), and C3 (green), belonging to, respectively, monomers D, A, and B. (B) Representation of the N-terminal (D1), central core (D2) and C-terminal (D3) domains of one enzyme subunit. Protein main polypeptide chain, represented as cartoon, is coloured in grey, and AMP and fumarate are represented as sticks and coloured as CPK. The illustration was generated with PyMOL (the PyMOL Molecular Graphics System, Version 1.8 Schrödinger, LLC).

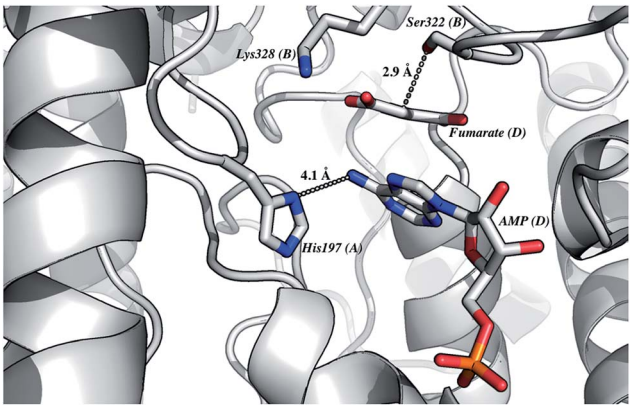

Fig. 3 The proposed residues involved in the reaction mechanism. This model of *Lb*ASL active site shows contacts of the imidazole side chain of His^{197} with AMP, and the putative catalytic base Ser^{322} with the C(β or α)-H of the succinyl moiety of the substrate. Protein main-chain, represented as cartoon, is coloured in grey, and AMP, fumarate and amino acid residues are represented as sticks and coloured as CPK. The illustration was generated with PyMOL (the PyMOL Molecular Graphics System, Version 1.8 Schrödinger, LLC).

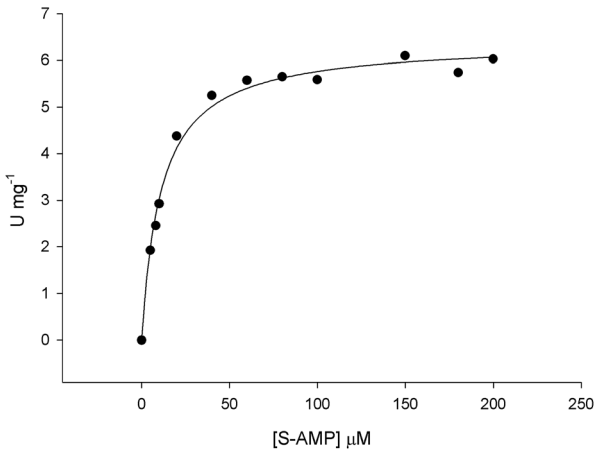

Fig. 4 Initial velocities for S-AMP conversion into AMP and fumarate. Substrate saturation curve was hyperbolic and data fitted to eqn (2).

Isothermal titration calorimetry (ITC)

As double reciprocal plots suggested a sequential kinetic mechanism for the reverse reaction, product binding to free enzyme was assessed by ITC to ascertain the order, if any, of chemical compound interaction with free *Lb*ASL. Accordingly, binary complex formation of either AMP or fumarate binding to free *Lb*ASL enzyme was studied by ITC. No heat change was detected upon addition of fumarate, suggesting that fumarate cannot bind to free *Lb*ASL enzyme (ESI, Fig. S4†). An exothermic profile (heat release) was observed for binary complex formation upon AMP binding to free *Lb*ASL protein (Fig. 6). The ITC data yielded the following values for *Lb*ASL:AMP binary complex formation: $\Delta H^{\#} = -5.5$ (± 1.5) kcal mol^{-1} and $\Delta S^{\#} = 3.13$ (± 0.84) cal mol^{-1} K^{-1}. The negative enthalpy value indicates a favorable, though small, redistribution of interactomic interactions network (*e.g.*, hydrogen bonds and/or van der Waals interactions) between the reacting species, including solvent. Hydrophobic interactions are related to the relative degrees of

Table 1 Steady-state kinetic parameters for S-AMP conversion into products catalyzed by ASL homologs

Specie	K_M (μM)	V_{max} (U mg^{-1})	k_{cat} (s^{-1})	k_{cat}/K_M (M^{-1} s^{-1})	Assay conditions
L. braziliensis	11.1 ± 0.9	6.4 ± 0.1	337 ± 5.4	3.0 (±0.2) × 10^7	25 °C pH 7.5
L. donovani (Spector *et al.*, 1979)	3.3 ± 0.5	100 ± 3	87.7 ± 2.6	2.7 (±0.4) × 10^7	30 °C pH 7.8
L. donovani (Boitz, *et al.*, 2013)	24.0	2.1	28	0.12 × 10^7	25 °C pH 7.0
P. falciparum (Bulusu *et al.*, 2009)	32.0 ± 1.6	—	7.5 ± 0.7	0.23 (±0.02) × 10^6	25 °C pH 7.4
H. sapiens (Lee and Colman, 2007)	1.78 ± 0.05	3.88 ± 0.07	3.40 ± 0.06	1.9 (±0.1) × 10^6	25 °C pH 7.4
M. smegmatis (Banerjee, 2014)	43.7 ± 2.6	—	0.70 ± 0.01	1.6 (±0.1) × 10^4	37 °C pH 7.6

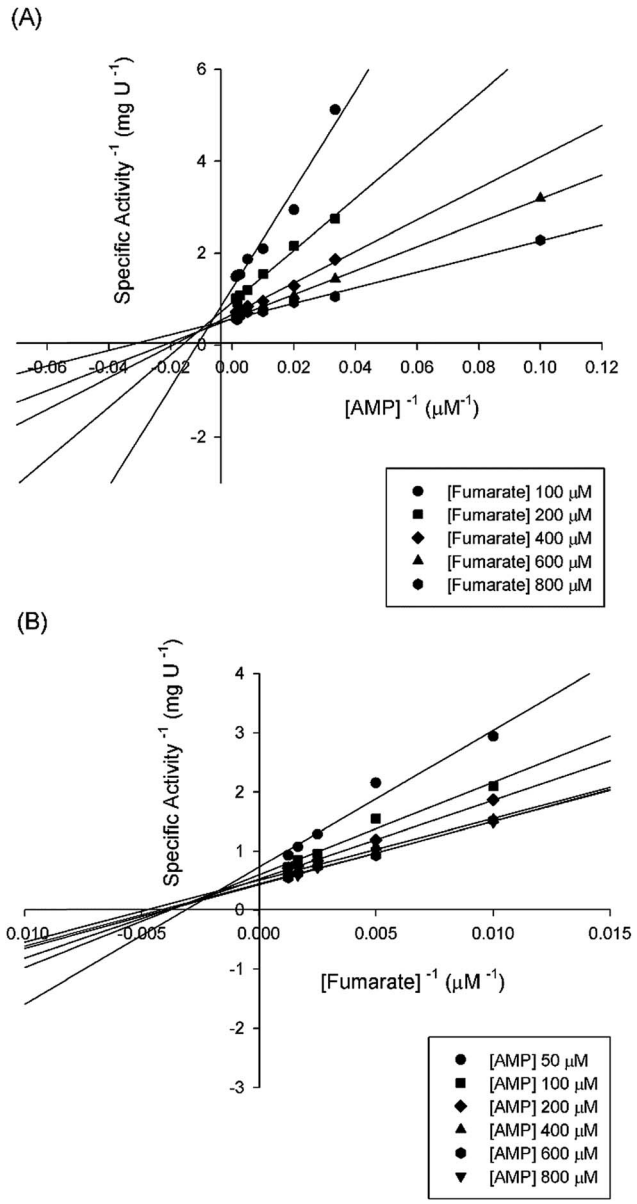

Fig. 5 Intersecting initial velocity patterns for ASL using either fumarate (a) or AMP (b) as the variable substrate. Each curve represents varied-fixed levels of the substrate.

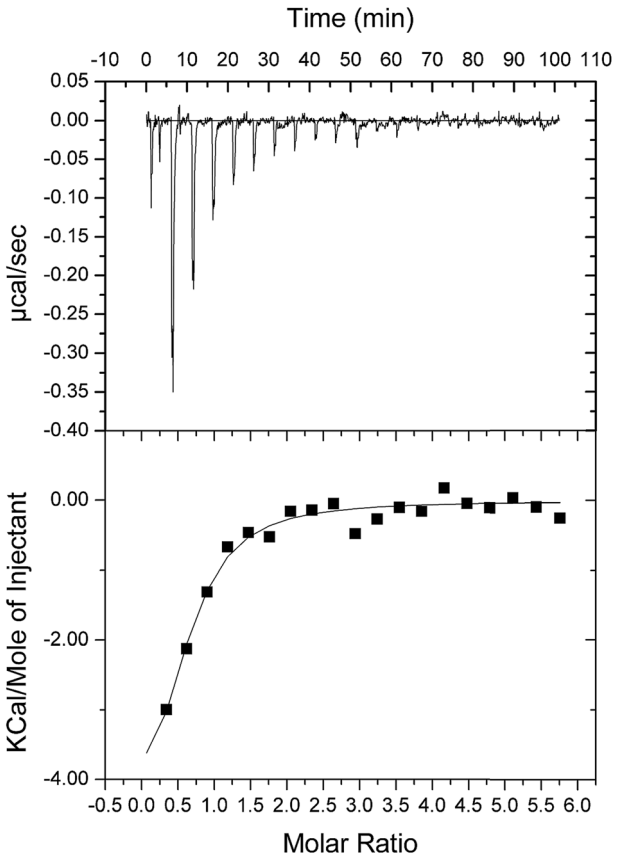

Fig. 6 ITC analysis of *Lb*ASL titration with AMP. The top panels show raw data of the heat pulses resulting from titration of *Lb*ASL. The button panels show the integrated heat pulses, normalized per mole of injection as a function of the molar ratio (ligand concentration/*Lb*ASL subunit concentration). Data were best fitted to a one binding site model.

disorder in the free and bound systems and thus these interactions are reflected in the entropy change. The release of "bound" water molecules from a surface to the bulk solvent is usually a source of favourable entropy (positive ΔS). A reduction in conformational states in either ligand or protein upon binary complex formation is entropically unfavourable (negative ΔS) because this molecular recognition process limits the external rotational and translational freedom of both partners (for instance, structuring regions of the protein adjacent to the bound ligand and loss of conformational freedom of free ligand).[45] The positive entropy value suggests either release of bound water molecules and/or an increase in conformational states in *Lb*ASL or AMP upon binary complex formation. The Gibbs free energy $\Delta G^{\#}$ value of −5.6 (±1.5) kcal mol^{-1} ($K_d \cong 19 \pm 7$ μM) suggests a favorable process for *Lb*ASL:AMP binary

complex formation. ITC data were fitted to one set of site binding model yielding a value of 0.6 (±0.1) for n (stoichiometry, ligands per active site). This result suggests that more than one subunit of *Lb*ASL contribute to AMP binding. Structural studies showed that three separate protomers contribute to each binding site of tetrameric *M. tuberculosis* ASL[39] and to other enzymes belonging to the aspartase/fumarase superfamily.[19] However, the stoichiometry should be equal to approximately one as there are four active sites per tetrameric *Lb*ASL enzyme.

The steady-state kinetic measurements for the reverse reaction and the ITC data for product binding to *Lb*ASL demonstrate that the reaction catalyzed by *Lb*ASL follows an ordered Uni-Bi kinetic mechanism, in which fumarate is the first product to dissociate from the ternary complex followed by AMP release to yield free enzyme for the next round of catalysis (Fig. 7). This proposal is in agreement with *L. donovani* ASL enzyme mechanism.[43]

Energy of activation

The energy of activation (E_a) for the *Lb*ASL-catalyzed chemical reaction was assessed by measuring the dependence of k_{cat} on temperature for S-AMP (Fig. 8). The E_a (6.8 ± 0.3 kcal mol^{-1}) of the reaction was calculated from data fitting to eqn (8) for the slope ($-E_a/R$) of the Ahrrenius plot (Fig. 8). The transition state enthalpy ($\Delta H^{\#} = 6.2 \pm 0.3$ kcal mol^{-1}), Gibbs free energy ($\Delta G^{\#} = 16.4 \pm 0.5$ kcal mol^{-1}) and entropy ($\Delta S^{\#} = -34.4 \pm 1.6$ cal mol^{-1} K^{-1}) at 25 °C were calculated using, respectively, eqn (9), (10) and (11). The E_a value of 6.8 kcal mol^{-1} represents the minimum energy needed to initiate the reaction, and the linearity of the Ahrrenius plot suggests that there is no change in the rate-limiting step over the temperature range employed (15–40 °C). The $\Delta G^{\#}$ value of 16.4 kcal mol^{-1} represents the energy barrier required for the reaction to occur and can be regarded as the variation of Gibbs energy between the enzyme–substrate activated complex and enzyme-substrate in the ground state.

The negative value for the entropy activation ($\Delta S^{\#}$) suggests that the entropy value for the enzyme:substrate activated complex is lower than the one for enzyme:substrate in the ground state, which may be accounted for by a loss of degrees of freedom on going from the ground state to activated state. The constant A (frequency factor that represents the frequency of collisions between reactant molecules) of eqn (8) corresponds to the product of collision frequency (Z) and the probability or steric factor (p) from the collision theory of reaction rates. From the absolute rate theory, $A = pZ = (k_B T/h)e^{\Delta S^{\#}/R}$. This equation enables us to interpret the probability factor (p) in terms of the molar entropy of activation ($\Delta S^{\#}$). If reactants are atoms or simple molecules, then relatively little energy is redistributed among the various degrees of freedom in the activated complex (transition-state complex). Consequently, $\Delta S^{\#}$ will be either a small positive or a small negative number, so that $\exp(\Delta S^{\#}/R)$ or p is close to unity. But if complex molecules are involved in a reaction, $\Delta S^{\#}$ will be either a large positive or a large negative number. In the former case, the reaction will proceed much faster than predicted by collision theory; in the latter case, a much slower rate will be observed. Note that the probability factor (p) takes into account the fact that in a collision complex molecules must be properly oriented to undergo the reaction (having the proper activation energy is a prerequisite but not a guarantee for a reaction to take place). Thus, the frequency factor (A) of the Arrhenius equation depends also on T and p (that accounts for that fact that colliding molecules must be properly oriented to undergo the reaction). The negative values for the entropy of activation ($\Delta S^{\#}$) for S-AMP reaction suggests that this reaction proceeds slower than predicted by the collision theory. Incidentally, a value of 17 466 582 ± 698 663 s^{-1} was obtained for A which allows to calculate an apparent first-order constant value of approximately 188 ± 8.2 s^{-1} using the Arrhenius equation ($k = Ae^{-E_a/RT}$), which is in reasonably good agreement with the k_{cat} value of 337 s^{-1} from steady-state kinetics data (Table 1).

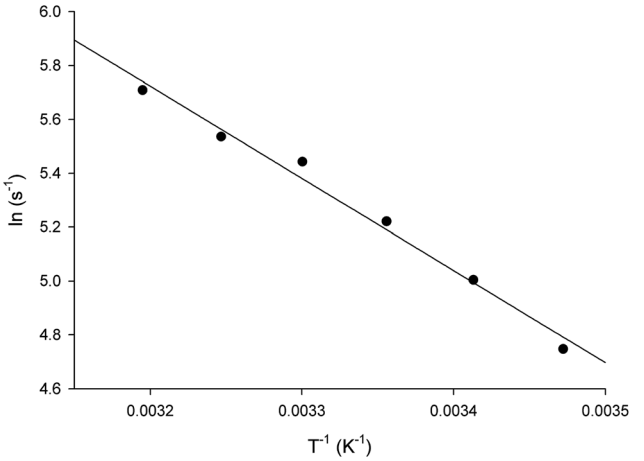

Fig. 8 Temperature dependence of ln k_{cat}. Saturating concentrations of S-AMP substrate were employed to measure the maximum velocity as a function of temperature ranging from 15 to 40 °C. The linearity of the Arrhenius plot suggests that there is no change in the rate-limiting step over the temperature range utilized in this assay.

Fig. 7 Proposed sequential ordered Uni-Bi kinetic mechanism for *Lb*ASL, in which fumarate release is followed by AMP dissociation to form free enzyme.

Solvent kinetic isotope effect (SKIE) and proton inventory

To evaluate the contribution of proton transfer from the solvent to a rate-limiting step of S-AMP conversion into fumarate and AMP for *Lb*ASL, SKIE were determined by data fitting to eqn (13) (Fig. 9), yielding a value of 1.40 ± 0.06 for ^{D_2O}V and of 1.20 ± 0.16 for $^{D_2O}V/K$. Isotope effects on V report on events following the ternary complex formation capable of undergoing catalysis (fully loaded enzyme), which include the chemical steps, possible enzyme conformational changes, and product release (leading to regeneration of free enzyme). Solvent isotope effects

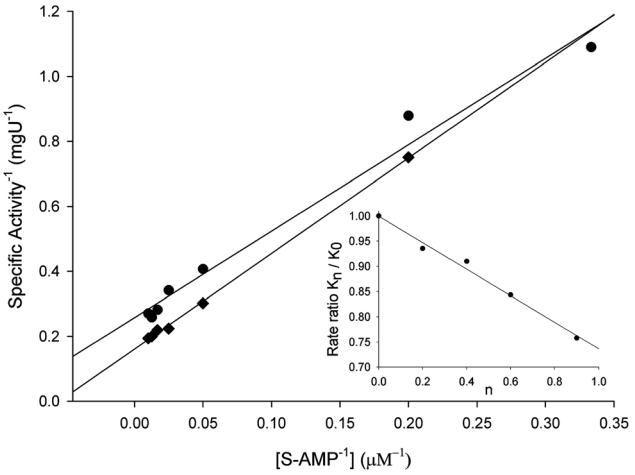

Fig. 9 Solvent kinetic isotope effects for *Lb*ASL. S-AMP was used as the variable substrate (5–100 μM). Reaction mixtures contained either 0 (◆) or 90 (●) atom % D_2O. The inset represents the proton inventory (0, 20, 40, 60 and 90 atom % D_2O) measuring *Lb*ASL enzyme activity at fixed-saturating concentration of S-AMP (100 μM), in which the *y*-axis represents the values for k_{cat} in solutions containing different mole fractions of D_2O (k_n) divided by k_{cat} in H_2O (k_0), and the *x*-axis gives the isotopic composition of the solvent (*n*).

on *V*/*K* report on the contribution of the proton transfer in steps in the reaction mechanism from binding of the isotopically labeled chemical compound (solvent) to the first irreversible step, usually considered to be the release of the first product (that is, all rate constants from reactant binding until the first irreversible step).[34] As rule of thumb, deuterium accumulates where binding is tighter (that is, fractionation factor is larger than one). Transition state proton contributes the reciprocal of its respective fractionation factor to the solvent isotope effect, whereas the contribution of a reactant state proton to the solvent isotope effect is equal to its fractionation factor.[34]

The values of *V*/*K* and *V* suggest that there is a modest contribution of solvent proton transference during the rate-limiting step of the reaction, probably events occurring after formation of the binary complex, as conformational and chemical changes. The proton inventory data show that the modest normal SKIE on *V* arises from a single protonic site (Fig. 9 inset). The SKIE on *V* data are similar to the results observed for *Pf*ASL.[44] On the other hand, there appears to be a modest normal SKIE effect on *V*/*K* for *Lb*ASL whereas no effect was observed for *Pf*ASL.[44] The latter suggests that subtle differences of substrate binding and solvent proton participation in this process may play a role in *Lb*ASL mode of action. Data fitting to eqn (14) yielded a transition state fractionation factor (φ^T) value of 0.74 ± 0.05, which is in agreement with the value observed for *Pf*ASL enzyme.[44] The transition state fractionation factor value suggests that binding of proton solvent to the transition state and/or to *Lb*ASL en route to catalysis is looser than the S-AMP substrate in the ground state and/or free enzyme as compared to bulk solvent. Solvation catalytic proton bridges are proton transfers that do not have appreciable proton motional amplitude in the reaction coordinate, but occur in stable, normal modes of the transition state.[34] Solvation catalytic proton bridges involve transfers among O, N, and S atoms, for which intrinsic free energy barriers are expected to be small compared to free-energy changes associated with covalent rearrangement of the heavy-atom (nonhydrogenic) framework of the reacting system. Hence, solvation catalytic bridges are strong H bonds with values φ^T values of 0.3–0.6.[34] The φ^T value thus suggests that solvent proton transfer in transition-state vibrations perpendicular to the reaction coordinate plays a role in *Lb*ASL mode of action. As these proton transfers are common for O and N, it is tempting to suggest that protonation of either His^{197}, His^{119}, Lys^{118}, Gln^{274}, Asn^{330} or Arg^{362} residues, proton transfer from Ser^{322} (or Lys^{118}) to N1/N6 of S-AMP may play a role in *Lb*ALS-catalyzed chemical reaction. However, it should be pointed out that solvent isotope effects lead to isotope exchanges at hundreds of protic positions of the enzyme, which precludes any assignment to a particular chemical group.

pH-rate profiles

In order to gain information on the chemical mechanism of *Lb*ASL and likely residues involved in catalysis and substrate binding, the dependence of kinetic parameters on varying pH values were determined. The pH-rate profile is shown in Fig. 10.

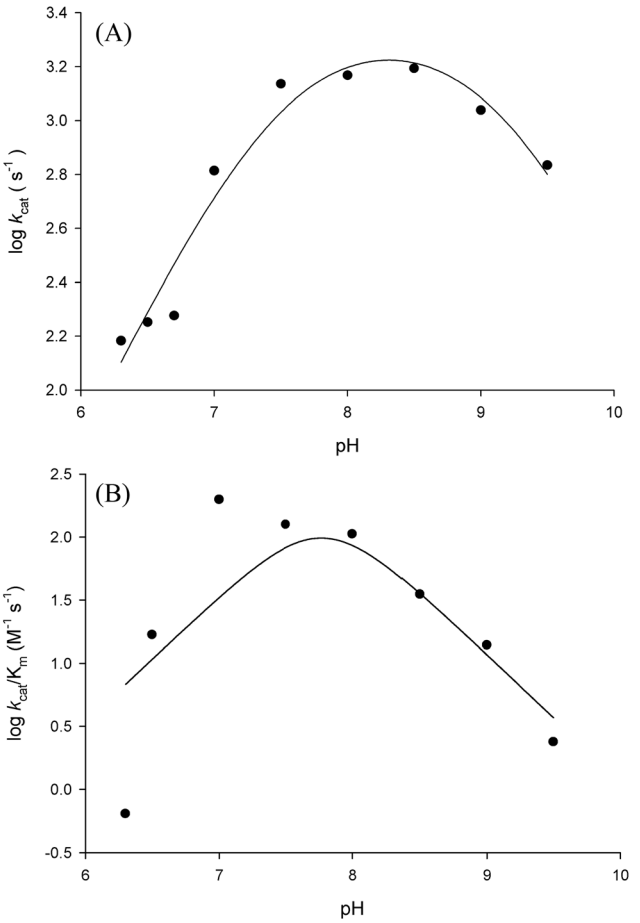

Fig. 10 Dependence of steady-state kinetic parameters on different pH values for *Lb*ASL reaction. (A) Data for pH dependence of log k_{cat} were fitted to eqn (15). (B) Data for the dependence of log k_{cat}/K_M on pH values were fitted to eqn (16).

The bell-shape pH-rate data for log k_{cat} were fitted to eqn (15) yielding apparent pK_a value of 7.5 ± 2.5 and pK_b value of 9.1 ± 4.9, which slopes of +1 for the acidic limb and −1 for the basic limb indicate the participation of a single ionizable group in each limb. This ionization could be occurring in either the substrate or enzyme.

It is propose that the cleavage of S-AMP to AMP and fumarate for ASL occurs through a general acid–base mechanism involving a β-elimination of fumarate. The reaction initiates by abstraction of the Cβ-proton from the substrate by the general base, resulting in the formation of a carbanion intermediate, and subsequent proton donation by the catalytic acid to the N1 or N6 atom of the substrate results in cleavage of the Cα–N bond and product release.[19,42] The His^{197} (for *Lb*ASL counting) is a highly conserved residue in the conserved region C2 in aspartase/fumarase superfamily. This histidine residue has being proposed to act as the general acid, donating a proton to the leaving group.[16,19] In previous site-direct mutagenesis studies, the mutation of correspondent His^{171} in *E. coli* ASL,[42] and His^{141} in *B. subtilis*,[41] (His^{197} in *Lb*ASL) showed decrease in enzyme activity, showing that these histidine residues play a role in catalysis. The His^{197} of *Lb*ASL may account for the apparent pK_a value of 7.5 in log k_{cat} analysis, which needs to be deprotonated for catalysis, whereas the pK value from the theoretical histidine imidazole group (pK = 6.0) could be shifted due interactions with others residues in the active site.

Another conserved region in the superfamily is flexible a Ser–Ser loop which plays an important role in catalysis, performing a conformational change from open to close conformation upon substrate binding in the active site. A lysine residue (Lys^{328} *Lb*ASL numbering) situated in the Ser–Ser loop, has been propose to interact with the α-carboxylate group of the substrate.[19] In addition, this lysine was suggested to be involved in the stabilization of the negative charge of the carbanion intermediate in *E. coli* ASL,[42] *E. coli* L-aspartase[46] and *E. coli* C-fumarase.[47] The apparent pK_b value of 9.1 may correspond to Ser^{322} (*Lb*ASL numbering), which could act as the catalytic base. Site-directed mutagenesis studies of the corresponding serines in *B. subtilis* and *H. sapiens* ASL proteins have shown that they are essential for catalysis.[48,49] Nevertheless, site-directed mutagenesis efforts will have to be pursued to ascertain the amino acid residues that play any role in catalysis.

Fitting the data of the rather complex pH-rate profile for k_{cat}/K_M (Fig. 10B) to either eqn (15) or (16) yielded poor estimates. For instance, data fitting to eqn (16) yielded pK values of 6.4 and 9.2 with large errors. The value of 9.2 likely corresponds to the same catalytic group implicated in catalysis by the pH-rate profile for k_{cat} (Fig. 10A). As pH-rate profile studies cannot differentiate between ionizable groups of enzyme and substrate(s), the two ionizing groups in the acidic limb (slope of +2) with a pK_a value of approximately 6.4 may correspond to either a protein amino acid residue or to the ionization of carboxyl groups of the succinyl moiety of S-AMP substrate whose dissociation constants may have been perturbed by the amino acid side chains of *Lb*ASL. However, caution should be exercised as the standard errors were rather large.

Conclusion

ASLs have been proposed as potential drug targets due to their important role in purine metabolism.[13,44,50,51] ASL is the last enzyme in the conversion of IMP to AMP. As *Leishmania* species lack the *de novo* pathway and are dependent on the salvage pathway to supply their purine requirements, *Lb*ASL could thus represent a drug target for the development of chemical agents to treat leishmaniasis. As point mutations in the human *purB* ASL-encoding gene causes autosomal recessive disorders such as autism, mental retardation, epilepsy and degeneration of muscles,[52–54] it is of paramount importance that species-specific enzyme inhibitor compounds be designed. Accordingly, exploiting differences in the mode of action between human ASL and enzyme from leishmania represents a promising approach to the design of anti-leishmiasis agents with limited host toxicity. The results presented here may contribute to a better understanding of the biology of *L. braziliensis*, and may aid to the development of *Lb*ASL enzyme inhibitors. Incidentally, it has recently been reported a promising vaccine candidate using a polyvalent α-Gal conjugate on Qβ virus-like nanoparticles that showed elimination of *Leishmania* infection and proliferation of parasites in a C57BL/6 α-galactosyltransferase knockout mouse model.[55] Although these preliminary results bode well, there have to be continuing efforts towards the development of alternatives strategies to combat *Leishmania* infection.

Author contributions

LG, PFD, CDR, ADV and LKBM designed, performed and analyzed all biochemical experiments, and drafted the paper. LFSMT and ONS built the molecular model and interpreted the structure of *Lb*ASL. CVB and ADV designed vectors, and performed cloning and expression. AFPM and CVB designed, performed and analyzed the mass spectrometry experiments. PB, EMCF, DSS and LAB designed experiments and revised critically the manuscript.

Conflicts of interest

The authors declare that they have no conflicts of interest with the contents of this article.

Acknowledgements

This work was supported by funds awarded by Decit/SCTIE/MSMCT-CNPq-FNDCT-CAPES to National Institute of Science and Technology on Tuberculosis (INCT-TB) to D. S. S. and L. A. B. L. A. B. (CNPq, 520182/99-5), D. S. S. (CNPq, 304051/1975-06), O. N. S. (CNPq, 305984/2012-8), and E. M. C. F. (CNPq, 306706/2014-8) are Research Career Awardees of the National Research Council of Brazil (CNPq). L. G. acknowledges a scholarship awarded by CAPES.

References

1 P. Kaye and P. Scott, Leishmaniasis: complexity at the host–pathogen Interface, *Nat. Rev. Microbiol.*, 2011, **9**, 604–615.
2 WHO, *Control of the leishmaniases: report of a meeting of the WHO Expert Committee on the control of Leishmaniases*, World Health Organization, Geneva, 2010.
3 J. Alvar, *et al.*, Leishmaniasis worldwide and global estimates of its incidence, *PLoS One*, 2012, **7**(5), e35671.
4 D. E. Teixeira, *et al.*, *Atlas didático Ciclo de vida da Leishmania*, Fundação CECIERJ, Consórcio CEDERJ, Rio de Janeiro, 2013.
5 L. H. Guimarães, *et al.*, Atypical manifestations of cutaneous Leishmaniasis in a region endemic for *Leishmania braziliensis*: clinical, immunological and parasitological aspects, *PLoS Neglected Trop. Dis.*, 2016, **10**(12), e0005100.
6 R. D. Azulay and D. R. Azulay Jr, Immune-clinical-pathologic spectrum of Leishmaniasis, *Int. J. Dermatol.*, 1995, **34**, 303–307.
7 S. L. Croft and G. H. Coombs, Leishmaniasis – current chemotherapy and recent advances in the search for novel drugs, *Trends Parasitol.*, 2003, **19**, 502–508.
8 S. L. Croft and P. Olliaro, Leishmaniasis chemotherapy - challenges and opportunities, *Clin. Microbiol. Infect.*, 2011, **17**, 1478–1483.
9 B. S. McGwire, *et al.*, Leishmaniasis: clinical syndromes and treatment, *Q. J. Med.*, 2014, **107**, 7–14.
10 A. Lemke, *et al.*, Amphotericin B, *Appl. Microbiol. Biotechnol.*, 2005, **68**, 151–162.
11 B. Chawla and R. Maghubala, Drug targets in Leishmania, *J. Parasit. Dis.*, 2010, **34**(1), 1–13.
12 J. J. Marr, *et al.*, Purine metabolism in *Leishmania donovani* and Leishmania braziliensis, *Biochim. Biophys. Acta*, 1978, **544**, 360–371.
13 J. M. Boitz, *et al.*, Adenylosuccinate synthetase and adenylosuccinate lyase deficiencies trigger growth and infectivity deficits in Leishmania donovani, *J. Biol. Chem.*, 2013, **288**(13), 8977–8990.
14 J. M. Boitz, *et al.*, Purine salvage in Leishmania: complex or simple by design?, *Trends Parasitol.*, 2012, **28**, 345–352.
15 R. L. Berens, *et al.*, Purine and Pyrimidine Metabolism, *Biochemistry and Molecular Biology of Parasites*, Academic Press Ltd, 1995, pp. 89–117.
16 E. A. Toth, *et al.*, The structure of adenylosuccinate lyase, an enzyme with dual activity in the *de novo* purine biosynthetic pathway, *Structure*, 2000, **8**, 163–174.
17 J. B. Palenchar, J. M. Crocco and R. F. Colman, The characterization of mutant *Bacillus subtilis* adenylosuccinate lyases corresponding to severe human adenylosuccinate lyase deficiencies, *Protein Sci.*, 2003, **12**, 1694–1705.
18 L. Z. Ariyananda and R. F. Colman, Evaluation of types of interactions in subunit association in *Bacillus subtilis* adenylosuccinate lyase, *Biochemistry*, 2008, **47**, 2923–2934.
19 V. V. Puthan, G. Fibriansah, H. Raj, A. W. H. Thunnissen and G. J. Poelarends, Aspartase/Fumarase superfamily: A common catalytic strategy involving general base-catalyzed formation of a highly stabilized *aci*-carboxylate intermediate, *Biochemistry*, 2012, **15**, 15–22.
20 New England BioLabs Inc, https://www.neb.com/protocols/0001/01/01/protein-expression-using-bl21de3-c2527, accessed November 2017.
21 R. C. Schwankea, *et al.*, Molecular cloning, expression in *Escherichia coli* and production of bioactive homogeneous recombinant human granulocyte and macrophage colony stimulating factor, *Int. J. Biol. Macromol.*, 2009, **45**, 97–102.
22 A. D. Villela, *et al.*, Biochemical Characterization of Uracil Phosphoribosyltransferase from Mycobacterium tuberculosis, *PLoS One*, 2013, **8**(2), e56445.
23 A. Shevchenko, H. Tomas, J. Havlis, J. V. Olsen and M. Mann, In-gel digestion for mass spectrometric characterization of proteins and proteomes, *Nat. Protoc.*, 2006, **1**(6), 2856–2860.
24 P. C. Carvalho, D. B. Lima, F. V. Leprevost, M. D. Santos, J. S. Fischer, P. F. Aquino, *et al.*, Integrated analysis of shotgun proteomic data with PatternLab for proteomics 4.0, *Nat. Protoc.*, 2016, **11**, 102–117.
25 J. K. Eng, T. A. Jahan and M. R. Hoopmann, Comet: an open source tandem mass spectrometry sequence database search tool, *Proteomics*, 2012, **13**, 22–24.
26 M. A. Larkin, G. Blackshields, N. P. Brown, R. Chenna, P. A. McGettigan, H. McWilliam, F. Valentin, I. M. Wallace, A. Wilm, R. Lopez, J. D. Thompson, T. J. Gibson and D. G. Higgins, Clustal W and Clustal X version 2.0, *Bioinformatics*, 2007, **23**, 2947–2948.
27 M.-Y. Shen and A. Sali, Statistical potential for assessment and prediction of protein structures, *Protein Sci.*, 2006, **15**, 2507–2524.
28 A. Sali and T. L. Blundell, Comparative protein modelling by satisfaction of spatial restraints, *J. Mol. Biol.*, 1993, **234**, 779–815.
29 V. B. Chen, W. B. Arendall, J. J. Headd, D. A. Keedy, R. M. Immormino, G. J. Kapral, L. W. Murray, J. S. Richardson and D. C. Richardson, MolProbity: all-atom structure validation for macromolecular crystallography, *Acta Crystallogr., Sect. D: Biol. Crystallogr.*, 2010, **66**, 12–21.
30 R. A. Laskowski, M. W. MacArthur, D. S. Moss and J. M. Thornton, PROCHECK: a program to check the stereochemical quality of protein structures, *J. Appl. Crystallogr.*, 1993, **26**, 283–291.
31 I. Segel, Enzyme Kinetics, *Behavior and Analysis of Rapid Equilibrium and Steady-State Enzyme Systems*, John Wiley and Sons, New York, 1975.
32 T. Lonhienne, E. Baise, G. Feller, V. Bouriotis and C. Gerday, Enzyme activity determination on macromolecular substrates by isothermal titration calorimetry: application to mesophilic and psychrophilic chitinases, *Biochim. Biophys. Acta*, 2001, **1545**, 349–356.
33 T. Lonhienne, E. Baise, G. Feller, V. Bouriotis and C. Gerday, Psychrophilic enzymes: revisiting the thermodynamic parameters of activation may explain local flexibility, *Biochim. Biophys. Acta*, 2000, **1543**, 1–10.

34 P. F. Cook, *Enzyme Mechanism from Isotope Effects*, CRC Press, Boca Raton, Florida, 1991.
35 P. F. Cook and W. W. Cleland, *Enzyme Kinetics and Mechanism*, Garland Science, London and New York, 2007.
36 P. Lee and R. F. Colman, Expression, purification, and characterization of stable, recombinant human adenylosuccinate lyase, *Protein Expression Purif.*, 2007, **51**, 227–234.
37 T. T. Lee, C. Worby, J. E. Dixon and R. F. Coman, Identification of His141 in the active site of *Bacillus subtilis* adenylosuccinate lyase by affinity labeling with 6-(4-Bromo-2,3-dioxobutyl)thioadenisine 5′-Monophosphate, *J. Biol. Chem.*, 1997, **272**, 458–465.
38 M. L. Segall and R. F. Colman, Gln212, Asn270, and Arg301 are critical for catalysis by adenylosuccinate lyase from Bacillus subtilis, *Biochemistry*, 2004, **43**, 7391–7402.
39 S. Banerjee, M. J. Agrawal, D. Mishral, S. Sharan, H. Balaram, H. S. Savithri and M. R. N. Murthy, Structural and kinetic studies on adenylosuccinate lyase from Mycobacterium *smegmatis* and *Mycobacterium tuberculosis* provide new insights on the catalytic residues of the enzyme, *FEBS J.*, 2014, **281**, 1642–1658.
40 W. A. Bridger and L. H. Cohen, The kinetics of adenylosuccinate lyase, *J. Biol. Chem.*, 1968, **243**, 644–650.
41 T. T. Lee, C. Worby, J. E. Dixon, Z. Bao and R. F. Colman, His68 and His141 are critical contributors to the intersubunit catalytic site of adenylosuccinate lyase of Bacillus subtilis, *Biochemistry*, 1999, **38**, 22–32.
42 M. Tsai, J. Koo, P. Yip, R. F. Colman, M. L. Segall and P. L. Howell, Substrate and product complexes of *Escherichia coli* adenylosuccinate lyase provide new insights into the enzymatic mechanism, *J. Mol. Biol.*, 2007, **370**, 541–554.
43 T. Spector, *et al.*, Specificity of adenylosuccinate synthetase and adenylosuccinate lyase from Leishmania donovani, *J. Biol. Chem.*, 1979, **254**, 8422–8426.
44 V. Bulusu, *et al.*, Elucidation of the substrate specificity, kinetic and catalytic mechanism of adenylosuccinate lyase from Plasmodium falciparum, *Biochim. Biophys. Acta*, 2009, **1794**, 642–654.
45 J. E. Ladbury and M. L. Doyle. *Biocalorimetry II*, Wiley, London, 2004.
46 S. Saribas, J. F. Schindler and R. E. Viola, Mutagenic Investigation of Conserved Functional Amino Acids in *Escherichia coli* L-Aspartase, *J. Biol. Chem.*, 1994, **269**(9), 6313–6319.
47 T. Weaver and L. Banaszak, Crystallographic Studies of the Catalytic and a Second Site in Fumarase C from *Escherichia coli*, *Biochemistry*, 1996, **35**, 13955–13965.
48 S. Sivendran and R. F. Colman, Effect of a new non-cleavable substrate analog on wild-type and serine mutants in the signature sequence of adenylosuccinate lyase of *Bacillus subtilis* and Homo sapiens, *Protein Sci.*, 2008, **17**, 1162–1174.
49 M. L. Segall, M. A. Cashman and R. F. Colman, Important roles of hydroxylic amino acid residues in the function of *Bacillus subtilis* adenylosuccinate lyase, *Protein Sci.*, 2007, **16**, 441–448.
50 T. Spector, R. L. Berens and J. J. Marr, Adenylosuccinate synthetase and adenylosuccinate lyase from Trypanosoma cruzi, Specificity studies with potential chemotherapeutic agents, *Biochem. Pharmacol.*, 1982, **31**, 225–229.
51 P. K. Fyfe, *et al.*, Structure of *Staphylococcus aureus* adenylosuccinate lyase (PurB) and assessment of its potential as a target for structure-based inhibitor discovery, *Acta Crystallogr., Sect. D: Biol. Crystallogr.*, 2010, **66**, 881–888.
52 J. Jaeken, S. Wadman, M. Duran, F. Van Sprang, F. Beemer, R. Holl, P. Theunissen, P. De Cock, F. Van den Bergh and M. Vincent, Adenylosuccinase deficiency: an inborn error of purine nucleotide synthesis, *Eur. J. Pediatr.*, 1988, **148**, 126–131.
53 P. Maaswinkel-Mooij, L. Laan, W. Onkenhout, O. Brouwer, J. Jaeken and B. Poorthuis, Adenylosuccinase deficiency presenting with epilepsy in early infancy, *J. Inherited Metab. Dis.*, 1997, **20**, 606–607.
54 D. Verginelli, B. Luckow, C. Crifo, C. Salerno and M. Gross, Identification of new mutations in the adenylosuccinate lyase gene associated with impaired enzyme activity in lymphocytes and red blood cells, *Biochim. Biophys. Acta*, 1998, **1406**, 81–84.
55 A. P. V. Moura, L. C. B. Santos, C. R. N. Brito, E. Valencia, C. Junqueira, A. A. P. Filho, M. R. V. Sant'Anna, N. F. Gontijo, D. C. Bartholomeu, R. T. Fujiwara, R. T. Gazzinelli, C. S. McKay, C. A. Sanhueza, M. G. Finn and A. F. Marques, Virus-like particle display of the α-Gal carbohydrate for vaccination against *Leishmania* infection, *ACS Cent. Sci.*, 2017, **3**, 1026–1031.
56 A. M. Waterhouse, J. B. Procter, D. M. Martin, M. Clamp and G. J. Barton, Jalview Version 2–a multiple sequence alignment editor and analysis workbench, *Bioinformatics*, 2009, **25**, 1189–1191.

